

RESEARCH

Open Access



Experimental Investigation on the Effect of Curing Condition and Admixture on Meso-Structure of Recycled Aggregate Concrete Based on X-ray CT

Yuzhi Chen^{1,2}, Yingjie Ning³, Xudong Chen², Weihong Xuan^{1*} and Yuzhu Guo²

Abstract

This study addresses the meso-structure of recycled aggregate concrete with different admixture and curing condition. The RCA (Recycled concrete aggregate) with admixture of slag powder and fly ash and curing condition of steam was casted. X-ray CT (Computed tomography) was used to obtain meso-structure of RCA, and the pore structure, aggregate, and interface traction zone were analyzed. The results show that steam curing not only increases the pore volume but also makes the pore morphology more complex, the fractal dimension increases, the proportion of spherical pores decreases, and the pores develop from spherical to flat and slender with the increase of steam curing temperature. The porosity of micron pores in recycled aggregate concrete is about 2.3%, in which the pores with aperture less than 300 μm accounts for more than 85%. The thickness of the interface area between recycled aggregate and new mortar is about 200 μm , and the crack width in recycled aggregate is about 300–400 μm .

Keywords: Steam curing, X-ray CT, Pore structure, Meso-structure, Fractal dimension

1 Introduction

The recycling of waste concrete into recycled aggregate (RA) not only reduces the environmental pressure caused by waste concrete but also greatly reduces the exploitation of natural resources (de Andrade Salgado & de Andrade Silva, 2022; Ma et al., 2022; Ouyang et al., 2022; Wang et al., 2022). However, because the RA is wrapped with the old mortar and has the characteristics of high crushing index and porosity, the incorporation of RA will cause the decrease of mechanical properties of concrete (Kou & Poon, 2008; McGinnis et al., 2017; Suryawanshi et al., 2015). The utilization rate of RA in China has been

at a low level, and RA is rarely used in concrete structural members. Under the background of building industrialization, the assembly of building components will become an important production mode of concrete structures. In the production process of prefabricated components, steam curing can improve the early strength of concrete, realize rapid demolding, and accelerate the turnover rate of formwork, which is the main measure for the prefabricated component production plant to improve production efficiency and economic benefits (Ramezaniapou et al., 2014; Shi et al., 2020a, 2020b). However, existing studies have shown that under high-temperature conditions, when the early strength is improved, the internal structure of concrete will also be imperfect, which will adversely affect the late strength and durability (Tan and Zhu, 2017; Shi et al., 2020a, 2020b). The influence of steam curing on the macroscopic mechanical properties and microstructure of concrete has long been the focus

Journal information: ISSN 1976-0485 / eISSN 2234-1315

*Correspondence: xwh@jit.edu.cn

¹ School of Architectural Engineering, Jinling Institute of Technology, Nanjing 211169, China

Full list of author information is available at the end of the article



© The Author(s) 2022. **Open Access** This article is licensed under a Creative Commons Attribution 4.0 International License, which permits use, sharing, adaptation, distribution and reproduction in any medium or format, as long as you give appropriate credit to the original author(s) and the source, provide a link to the Creative Commons licence, and indicate if changes were made. The images or other third party material in this article are included in the article's Creative Commons licence, unless indicated otherwise in a credit line to the material. If material is not included in the article's Creative Commons licence and your intended use is not permitted by statutory regulation or exceeds the permitted use, you will need to obtain permission directly from the copyright holder. To view a copy of this licence, visit <http://creativecommons.org/licenses/by/4.0/>.

of researchers in this field (Gonzalez-Corominas et al., 2016; Jun et al., 2012).

Li et al. (2017) studied and compared the influence of steam curing temperature and time on the performance of concrete containing a large amount of fly ash or slag powder. Compared with prolonging steam curing time, increasing temperature is more beneficial to fly ash concrete. When steam curing at 80 °C, fly ash and slag reduce the damage risk of delayed ettringite on the microstructure of concrete. The effect of fly ash on improving pore structure and enhancing chloride ion permeability is better than that of slag. Yang et al. (2021) studied the effects of fineness and content of fly ash and curing system on the compressive strength and microstructure of steam-cured high content fly ash cement composites. Ultrafine fly ash can improve the early and late strength of steam-cured composites, and effectively improve the pore structure of composites. Compared with prolonging steam curing time, increasing temperature seems to be more effective in fusing aluminum in fly ash into calcium silicate hydrate. Hong et al. (2006) studied the influence of slag on the strength and microstructure of steam curing ordinary Portland cement concrete. Increasing the content of slag increases the compressive strength of concrete and improves the microstructure to enhance the permeability and freeze–thaw resistance. Kim et al. (2011) studied the applicability of slag in shield lining and found that replacing 50% ordinary cement with slag was the optimum mixing condition. Compared with standard curing, when steam curing at 60 °C for 4 h, not only the early strength increased by more than 3 times but also the 28-day strength increased by about 30%.

Lee et al., (2005a, 2005b) tested the mechanical properties and chloride ion penetration of steam-cured recycled aggregate concrete (RAC). When the replacement rate of recycled coarse aggregate does not exceed 50%, the strength and chloride ion permeability are within a reasonable range, which is close to that of ordinary concrete. The RAC can be used for structural members when the content of RA is controlled. Poon et al. (2006) studied the influence of steam curing on the mechanical properties and pore structure of RAC. Steam curing improved the 1-day strength of concrete, but the 28-day and 90-day strength were lower than that of water curing. The static elastic modulus of concrete

also decreased, but the negative impact of steam curing decreased with the increase of RA content. Steam curing can improve the compactness and anti-chloride ion permeability of RAC. The research shows that steam curing is a practical method to increase the content of RA.

The recycled aggregate has defects, and the steam curing system causes thermal damage to concrete. Therefore, a large number of mineral admixtures are used to inhibit the thermal damage of concrete during steam curing. However, previous studies mainly focused on the influence of recycled aggregate concrete or steam curing system on the microstructure of concrete, and less on the influence of large mineral admixtures on steam curing system concrete. In order to explore the mechanism of the influence of steam curing on the macro mechanical properties of RAC mixed with slag and fly ash, the microstructural characteristics of RAC with different steam curing systems, such as porosity, pore size distribution, and pore structure morphology, were analyzed by CT scanning technique.

2 Test Scheme

2.1 Materials

The cement used in the test is P.O 42.5 ordinary Portland cement, and the admixtures are low calcium fly ash and S95 blast furnace slag powder. The specific surface areas of cement, fly ash, and slag are 378 m²/kg, 365 m²/kg, and 420 m²/kg, respectively. The 3-day steam curing activity indexes of slag powder and fly ash were 106.9% and 78.1%, and the 28-day steam curing activity indexes were 119.4% and 90%, respectively. The chemical composition of cement, slag powder, and fly ash is shown in Table 1.

The aggregate gradation curve is shown in Fig. 1. The maximum nominal particle size of RA is 26.5 mm, the bulk density is 1264.5 kg/m³, the water absorption is 4.9%, and the crushing index is 15.2%. The fine aggregate is natural river sand with fineness modulus of 2.5. According to the comparison between the recycled aggregate and the natural aggregate, the recycled aggregate has a large particle size and a single particle size distribution, which indicates that the surface of the recycled aggregate is covered by old mortar and is not completely broken.

Table 1 Chemical composition of cementitious materials (%)

Component	CaO	MgO	SiO ₂	Fe ₂ O ₃	P ₂ O ₅	Al ₂ O ₃	SO ₃	LOI
Cement	54.65	2.58	22.07	4.32	1.03	6.30	2.59	2.14
Fly ash	8.18	0.30	41.11	6.28	1.15	38.62	0.42	3.61
Slag powder	45.09	6.99	27.33	0.45	0.13	13.66	4.03	0.95

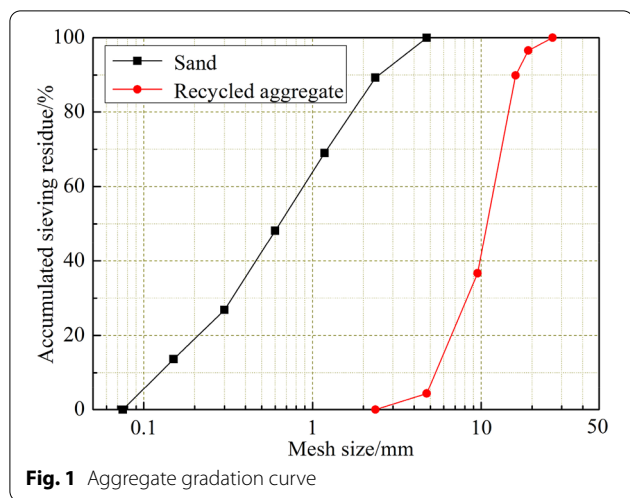


Fig. 1 Aggregate gradation curve

2.2 2.2 Mix Proportion

Three test blocks shall be prepared for each test group, and each material shall be weighed according to the design mix proportion. Before mixing the recycled aggregate concrete, the recycled aggregate shall be treated by means of pre-water absorption to make it reach the saturated surface dry state, and then the recycled aggregate shall be used for mixing. Coarse aggregate, sand, cement, slag powder, and fly ash shall be manually mixed for 1 min, and then the concrete mixer shall be used for dry mixing for 2 min. After ensuring that all materials are fully contacted, the mixing water shall be added to continue mixing for 2 min, and then the vibrating table shall be used for vibration and molding. In the test, 50% cement is replaced by slag powder or mixed slag powder and fly ash, in which the ratio of slag powder to fly ash is 3:2. The water absorption of RA used in this work was 4.9%. The mixture of RAC is shown in Table 2, in which the sample numbers of RACC, RACS, and RACSF represent that cementitious materials with all ordinary Portland cement, 50% slag powder, and 30% slag powder + 20% fly ash, respectively. And the water cement ratio is 0.3, sand ratio is 0.46. The polycarboxylic acid high-performance water reducing agent was used, and the content is 0.7% of the cementitious material. The concrete mixtures have good fluidity, and the slump is between 190 and 200 mm.

Table 2 Mix proportion of recycled aggregate concrete (kg/m³)

No	Cement	Slag powder	Fly ash	Sand	RA	Water	PCA
RACC	483	0	0	815	957	145	3.42
RACS	241.5	241.5	0	815	957	145	3.42
RACSF	241.5	144.9	96.6	815	957	145	3.42

2.3 Curing condition

In this paper, there are two different curing condition was considered. On one hand, RACC, RACS, and RACSF were cured in the standard environment (temperature of 20 ± 2 °C and humidity of 95%) after casting tested at the age of 28 days, respectively. On the other hand, RACS was curing with steam. The steam quick curing box is used for steam curing, which can programmatically control the curing temperature and time. The steam curing process of concrete can be divided into static stage, heating stage, constant temperature stage, and cooling stage. The curing temperature and holding time of the test are shown in Table 3. The static stage starts from the pouring of concrete into the test mold, and the concrete was placed in the test mold for 3 h at 20 °C. The heating stage is 2 h from 20 °C to the target steam curing temperature. The duration of the cooling phase is 2 h, from the steam curing temperature to 20 °C. Two steam curing systems are adopted: steam curing at 60°C for 12 h and steam curing at 80°C for 9 h, which are recorded as ‘6012’ and ‘8009’, respectively. For example, Fig. 2 shows the time–history curve with curing temperature of 60°C and holding time of 12 h. After the steam curing, the specimens were demolded and placed in the standard curing environment for testing at 28 days. The mechanical properties of each mix are tested and the results are listed in Table 4.

2.4 X-Ray CT

The German Vtomexs micro-focus X-ray CT system (Fig. 3) was used in the test. The maximum tube power of the system is 320 W, the X-ray source voltage range was 10~240 kV, and the tube head current range of the equipment was 0.01–3.0 mA. The scanned sample is a cylinder with a diameter of 50 mm and a height of

Table 3 Steaming system parameters

Sample No	Static time /h	Heating time /h	Curing temperature /°C	Holding time /h	Cooling time /h
RACS-6012	3	2	60	12	2
RACS-8009			80	9	

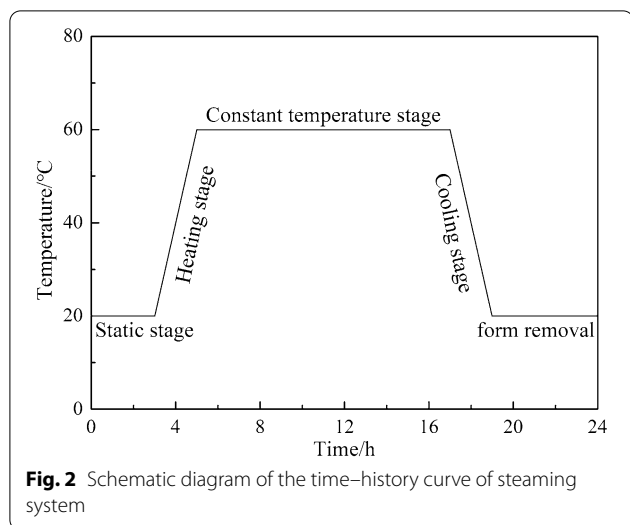


Fig. 2 Schematic diagram of the time–history curve of steaming system

Table 4 Steaming system parameters

Sample No	RACC	RACS	RACSF	RACS6012	RACS8009
Compressive strength	59.6	61.4	51.9	56.7	54.6

100 mm, and the image resolution is 59.2 μm/voxel, and the number of pixels in the image is 1024 × 1024. The 2D slice image of the sample is obtained by scanning and the first step of image post-processing is to distinguish the gray range of pores, aggregates, and mortar according to the gray value.

Fig. 4 shows the determination process of gray value range of each component of recycled aggregate concrete. Firstly, a line segment is drawn at position with recycled aggregate, new mortar, old mortar, and pore in the 2D CT slice image, as shown in Fig. 4a. Fig. 4b shows the

gray values of different phase of different components. It can be found that gray value range of each phase is obviously different, and new mortar, coarse aggregate, old mortar, and pore with gray values of 6400, 5450, 7000, and 2400 can be used to threshold segmentation, respectively. According to Fig. 4b, when the gray value is less than 2400, it can be identified as pore, and when the gray value range is 2400–5400, it can be identified as old mortar. Then, the three-dimensional reconstruction of each component can be carried out by AVIZO software. Finally, the three-dimensional structure of the reconstruction can be analyzed. The stack image is obtained through CT, and the 3D model reconstruction is realized by using the commercial software VG Studio. Fig. 5 shows the three-dimensional model of each phase structure of the reconstructed concrete after segmentation, in which the corresponding structures of each number are as follows: (1) aggregate; (2) pore; (3) new mortar; (4) old mortar; and (5) total model.

3 Results and Discussion

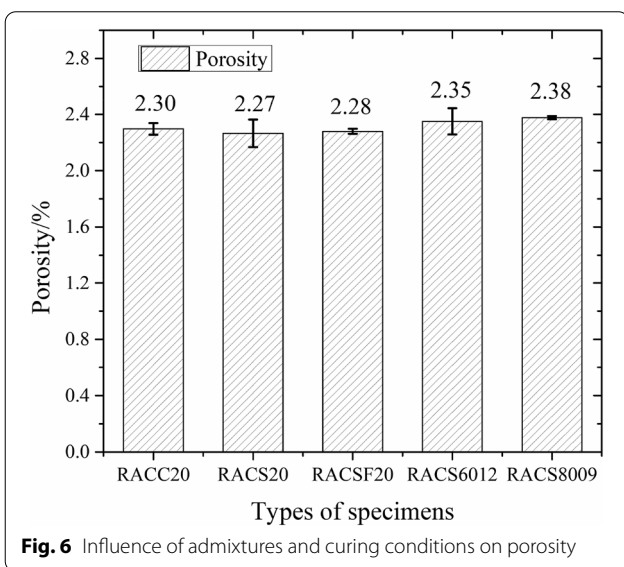
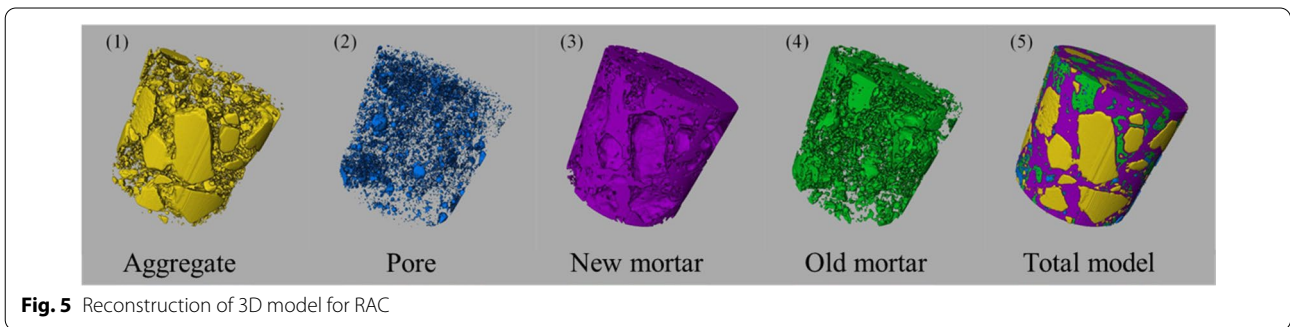
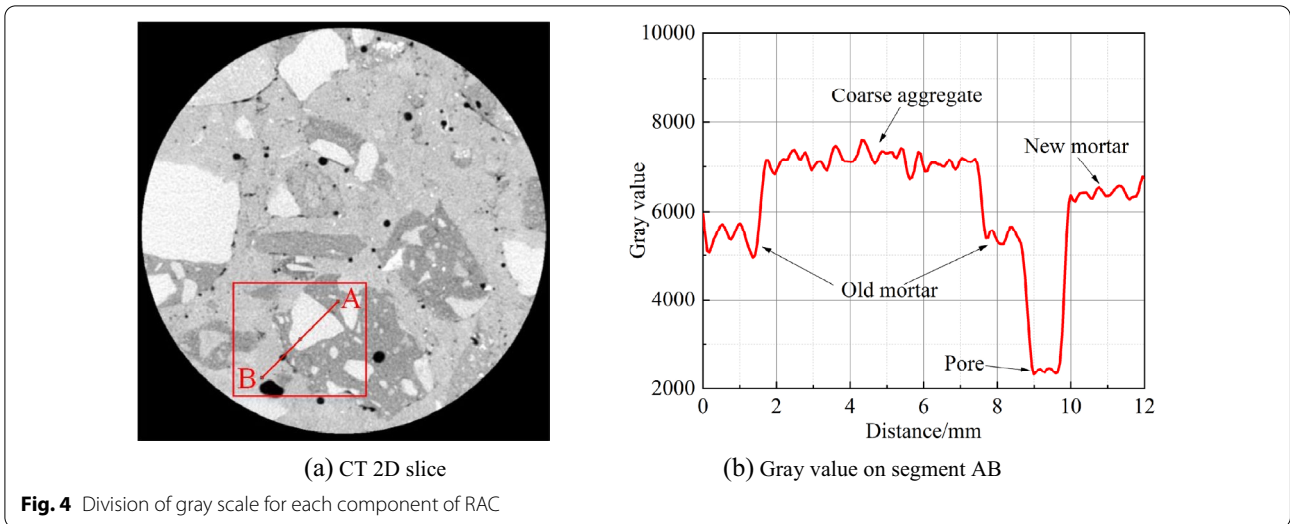
3.1 Characteristic Analysis of Pore Structure

3.1.1 Porosity and Pore Size Distribution

To analyze the influence of steam curing and admixtures on the pores of RAC, a statistical analysis of the porosity and pore size distribution is carried out. Fig. 6 shows the porosity of different specimens. It can be seen that the porosity of each specimen is relatively close, between 2.27% and 2.38. The addition of slag powder and fly ash reduced the porosity slightly, while the high-temperature steam curing increased the porosity. The pore size distribution is shown in Fig. 7 as percentage value and cumulative percentage value, respectively. The proportion of pores with a pore diameter of 75–300 μm reaches more than 85%. Fig. 7 shows that responses are basically the same which indicates that the addition of a large number



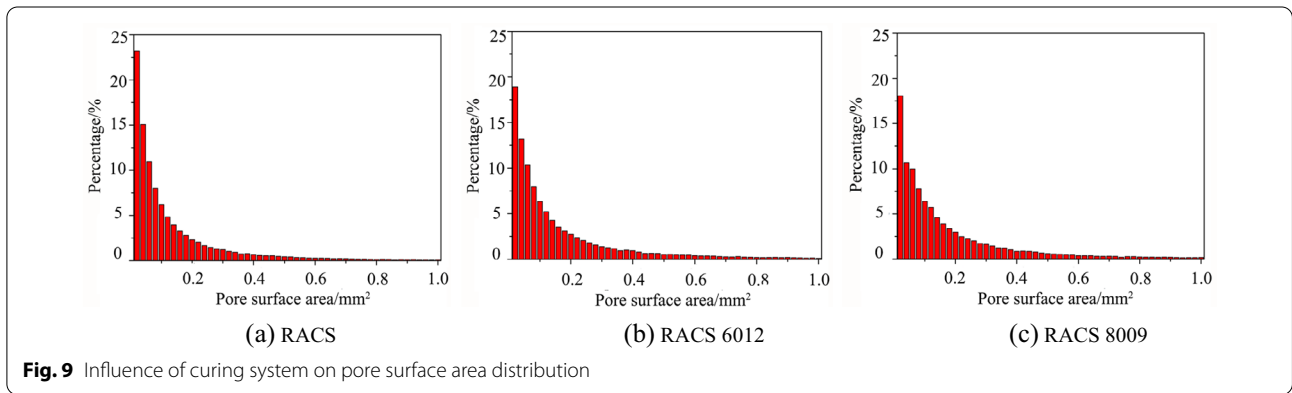
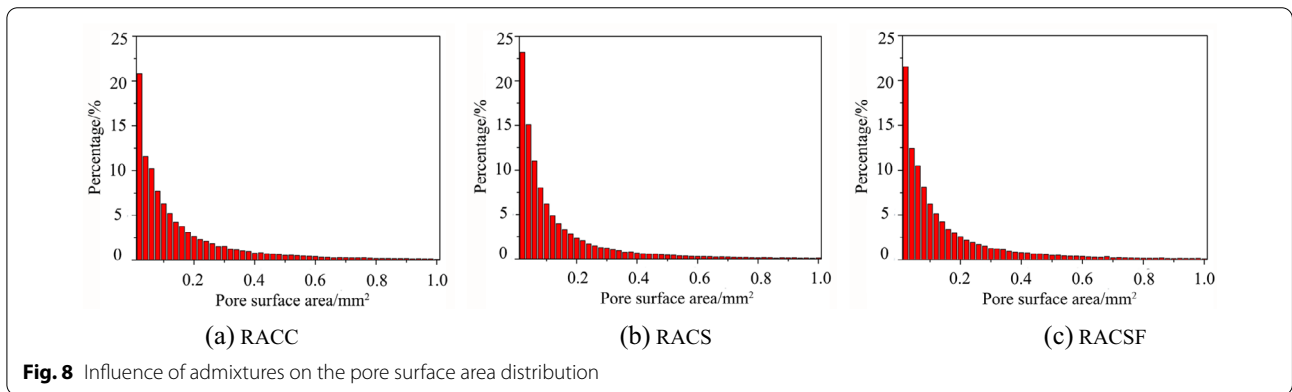
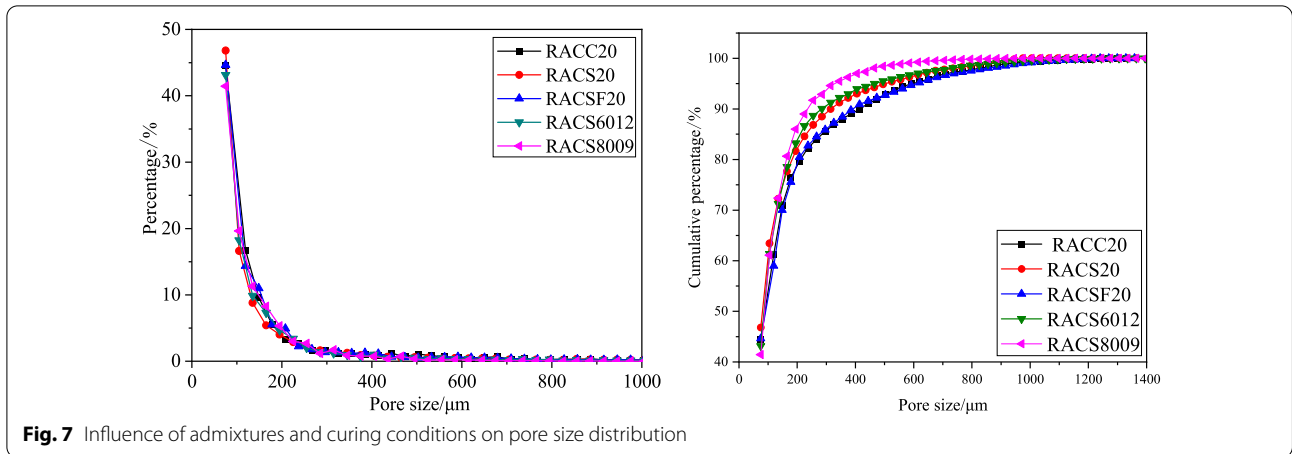
Fig. 3 X-CT scanning equipment



of mineral admixtures, and the high-temperature steam curing conditions promote the pozzolanic effect of slag powder and fly ash and generate more C-S-H gel in a short time, thus reducing the thermal damage caused by steam curing system. Hu et al. cleared that if the replacement amount of fly ash exceeds a certain high proportion (70%), the value of open porosity tends to decrease regardless of the curing conditions are diverse.

3.1.2 Distribution of Pore Surface Area

Pore surface area is a comprehensive reflection of pore diameter and pore shape. The smaller the pore diameter, the fuller the shape, and the smaller the pore surface area. It can be seen from Fig. 7 that the pore diameter is less than 300 μm is dominant. The pores with a surface area of 0–1 mm² are divided at intervals of 0.02 mm² to obtain the distribution of pore surface

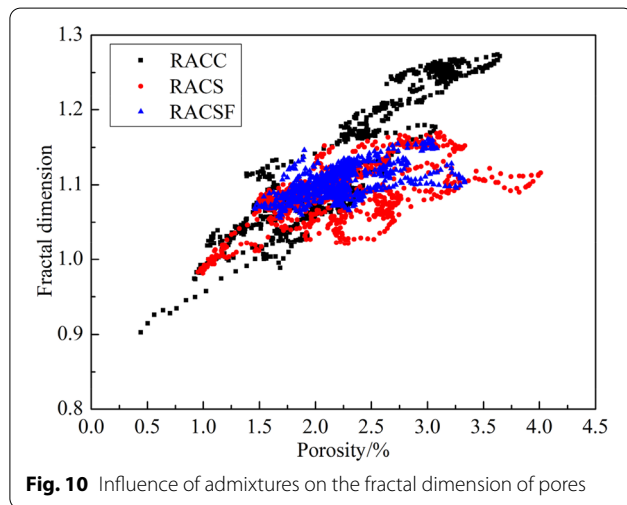
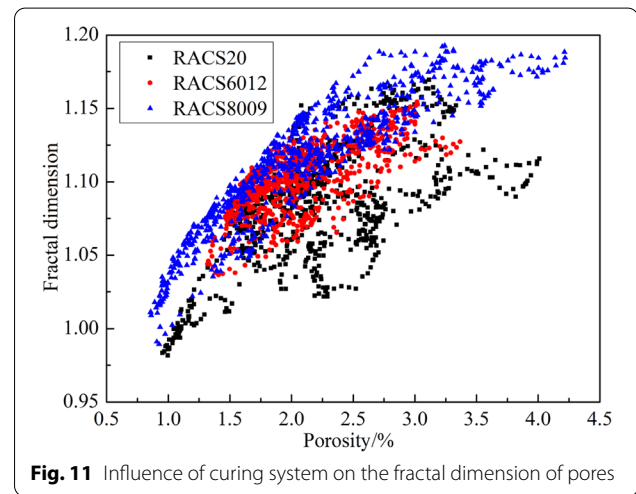


area, as shown in Figs. 8 and 9. Statistical results of the pore surface area are listed in Table 5. The pore surface area less than 0.6 mm^2 accounts for more than 90%. In the composite system, small particles will fill the pores of large particles, and the filling effect between small

and large particles will appear, which will reduce the porosity and increase the compactness. It can be seen from the figure that the addition of slag powder and fly ash can refine the pores and increase the proportion of small holes, while the proportion of small holes in high-temperature steam-cured specimens decreases.

Table 5 Percentage value of pore surface area in different ranges (%)

Range of pore surface area/ mm ²	0–0.1	0.1–0.2	0.2–0.4	0.4–0.6	0.6–0.8	0.8–1.0
RACC20	56.57	18.92	14.41	5.72	2.76	1.63
RACS20	63.42	17.20	11.82	4.28	2.07	1.20
RACSF20	58.78	18.26	13.53	5.27	2.56	1.60
RACS6012	52.90	20.52	15.82	6.12	2.89	1.76
RACS8009	58.78	18.26	13.53	5.27	2.56	1.60

**Fig. 10** Influence of admixtures on the fractal dimension of pores**Fig. 11** Influence of curing system on the fractal dimension of pores

3.1.3 Pore Fractal Dimension

To further analyze the influence of steam curing and admixtures on the pore structure shape of RAC, taking the two-dimensional slices of concrete specimens as samples, the two-dimensional fractal dimensions of the pores of five groups of specimens RACC20, RACSF20, RACS20, RACS6012, and RACS8009 were analyzed and calculated. The box counting method (Liu et al., 2016) is used to calculate the fractal dimensions of the two-dimensional slices, as shown in Eq. (1):

$$D = \lim_{r \rightarrow 0} \frac{\log N(r)}{\log(r)}, \quad (1)$$

where r is the edge length of lattices divided on slices and N is the number of lattices.

The fractal dimension calculation results are combined with the two-dimensional porosity to draw the scatter diagram, as shown in Figs. 10 and 11. In the figure, the x -axis is the percentage of pores on each slice, that is, the two-dimensional porosity. There are 800 slices in total, and the porosity changes in the range of 1–4%. The average value of the two-dimensional porosity of all slices is calculated. The two-dimensional average porosity of

the five groups of specimens is between 2.1% and 2.3%, which is close to the 3D porosity in Fig. 6. It can be seen from Fig. 10 that the addition of slag powder and fly ash reduces the fractal dimension of the pores and optimizes the pore shape. This is because the mineral admixture is smaller than the cement particle size, so it can fill the gap and make the mixture achieve the optimization of the skeleton. The more complex the particle size distribution, the higher the compactness, and the smaller the fractal dimension. The effect of steam curing conditions on the fractal dimension of the specimen is also obvious, as shown in Fig. 11. With the increase of steam curing temperature, the fractal dimension of pores increases significantly, indicating that steam curing makes thermal damage leading to the pore structure morphology in the concrete more complex.

3.1.4 Pore Sphericity

Sphericity is an important parameter to quantitatively characterize the pore shape in concrete. Its physical meaning is the ratio of the surface area of a sphere with the same volume as the pore to the surface area of the pore. The calculation is shown in Eq. (2) (Guo et al., 2021):

$$\psi = \frac{\sqrt[3]{\pi(6V)^2}}{A}, \tag{2}$$

where V is the pore volume (mm^3) and A is the pore surface area (mm^2).

The closer the sphericity is to 1, the closer the pore shape is spherical. If the sphericity of the pore structure is poor, it is easy to generate local stress concentration at the edge of the pore, which adversely affects the mechanical properties and durability of the concrete. To further analyze the influence of steam curing and admixtures on the pore sphericity of RAC, the distribution of pore sphericity of five groups of specimens RACC20, RACSF20,

RACS20, RACS6012, and RACS8009 were counted. Figs. 12 and 13 show the effect of admixture and steam curing on pore sphericity, respectively. The percentage value of pore sphericity in different ranges is provided in Table 6. It can be seen that the frequency of pore sphericity is the highest within the range close to 1. Adding slag powder and fly ash increases the proportion of sphericity close to 1. The proportions of RACC20, RACSF20, and RACS20 with sphericity close to 1 are 34.59%, 38.41%, and 36.59%, respectively. Furthermore, the proportion of pores with sphericity of 1 in RACS6012 and RACS8009 specimens was 36.61% and 32.51%, respectively. Steam curing has an adverse effect on the sphericity of the

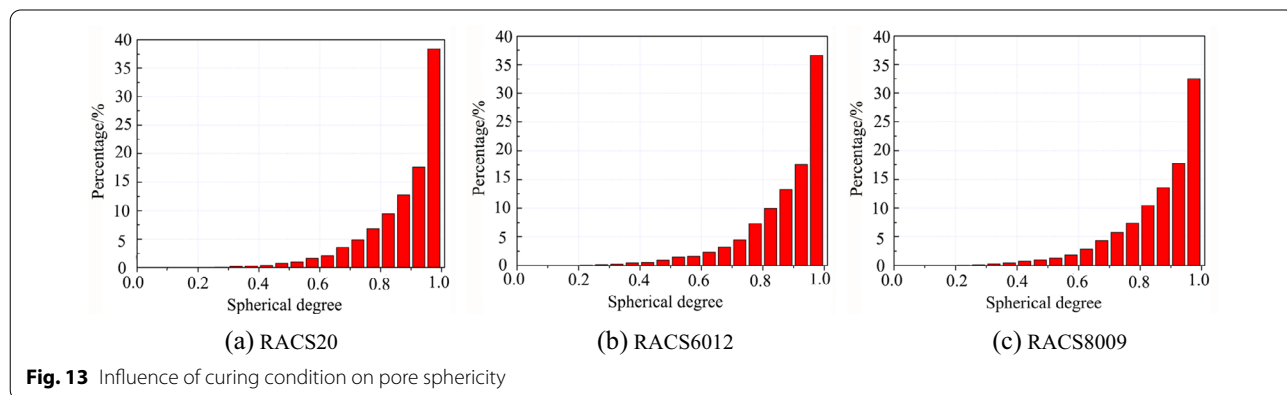
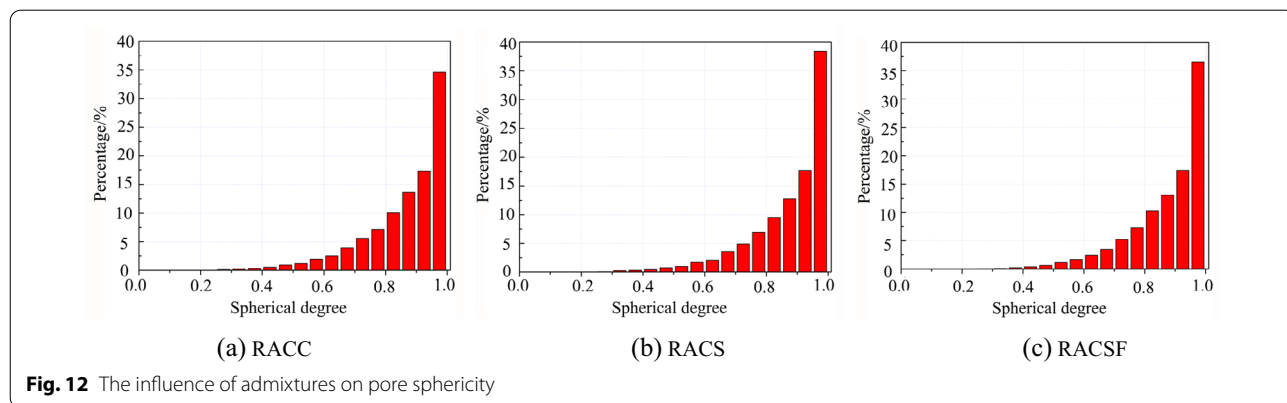


Table 6 Percentage value of pore sphericity in different ranges (%)

Pore sphericity	0–0.275	0.275–0.475	0.475–0.675	0.675–0.825	0.825–0.925	0.925–0.975
RACC20	0.17	1.99	9.50	22.79	30.94	34.59
RACS20	0.096	1.66	8.26	21.18	30.39	38.41
RACSF20	0.094	1.38	8.70	22.76	30.47	36.59
RACS6012	0.23	2.09	8.59	21.71	30.76	36.61
RACS8009	0.19	2.30	10.24	23.55	31.21	32.51

Table 7 Classification of shape factor index

Classification	Stretch ratio	Flatness ratio	Shape
I	>0.67	<0.67	Pie
II	>0.67	>0.67	Spherical
III	<0.67	<0.67	Bladed
IV	<0.67	>0.67	Rod

Table 8 Statistics of the proportions of the four types of pores in different specimens

Sample No.	Pie (%)	Spherical (%)	Bladed (%)	Rod (%)
RACC20	15.18	20.46	47.51	16.83
RACS20	16.13	22.31	43.38	18.18
RACSF20	15.95	23.17	42.20	18.68
RACS6012	16.32	21.08	42.71	19.89
RACS8009	14.92	12.95	53.35	18.78

pores. With the increase of steam curing temperature, the proportion of sphericity of 1 decreased, especially the sphericity of concrete after steam curing at 80 °C–9 h became worse. Therefore, high-temperature steam curing leads to poor sphericity of internal pores of concrete, which may be one of the reasons for the reduction of concrete compressive strength.

3.1.5 Pore Shape Factor

In order to further explore the change of pore sphericity due to steam curing, the pore morphology of concrete samples was analyzed by shape factor parameter (Chandrappa & Biligiri, 2018). The shape factor is an indicator to measure the pore shape based on the ratio elongation and flatness of three-dimensional dimension. The ratio of 0.67 was taken as the dividing line, and the pores in concrete are divided into pie shaped, spherical, blade shaped, and rod shaped [21]. The larger the ratio, the fuller the pore shape. The smaller the single ratio or both ratios, the

more flattened and elongated the pores. The classifications of shape factor index are shown in Table 7.

The shape factor analysis method is used to statistically analyze the pore shape in RAC specimens. The statistics of the proportions of the four types of pores in different specimens in Table 8. It can be seen that the pore shape in RCA is mainly blade shaped and spherical. As shown in Fig. 14, with the addition of fly ash and slag powder, the number of concrete pores in Area II increases gradually, indicating that under standard curing conditions, adding slag powder and fly ash optimizes the pore shape and slightly increases the proportion of spherical pores. However, steam curing, especially at high temperature, has a significant impact on the pore shape. As shown in Fig. 15, steam curing system makes pore shape more regional III compared with standard curing, 80 °C steam curing reduces the proportion of spherical pores by 9.36% and increases the proportion of leaf-shaped pores by 9.97%.

3.2 Recycled Aggregate Characterization

3.2.1 Composition and Percentage of Recycled Aggregate

The recycled aggregate surface is attached with the old mortar in the original concrete, the quality of the old mortar is uneven, and its performance is obviously different from that of the aggregate, which should be distinguished from the aggregate. This virtually reduces the real content of the aggregate in the recycled aggregate concrete, which will inevitably have a certain impact on the performance of the concrete.

According to the threshold segmentation results of two-dimensional slice of CT scanning, the ratio of the area occupied by recycled aggregate (aggregate+old mortar), aggregate and old mortar on the two-dimensional slice to the cross-sectional area of the whole specimen is defined as their respective percentages. The specific expression of aggregate percentage is shown in Eq. (3):

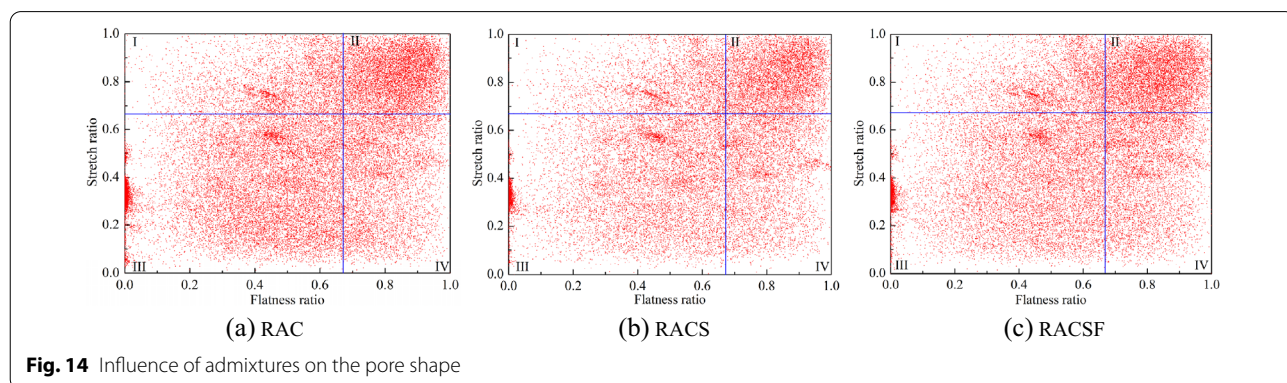


Fig. 14 Influence of admixtures on the pore shape

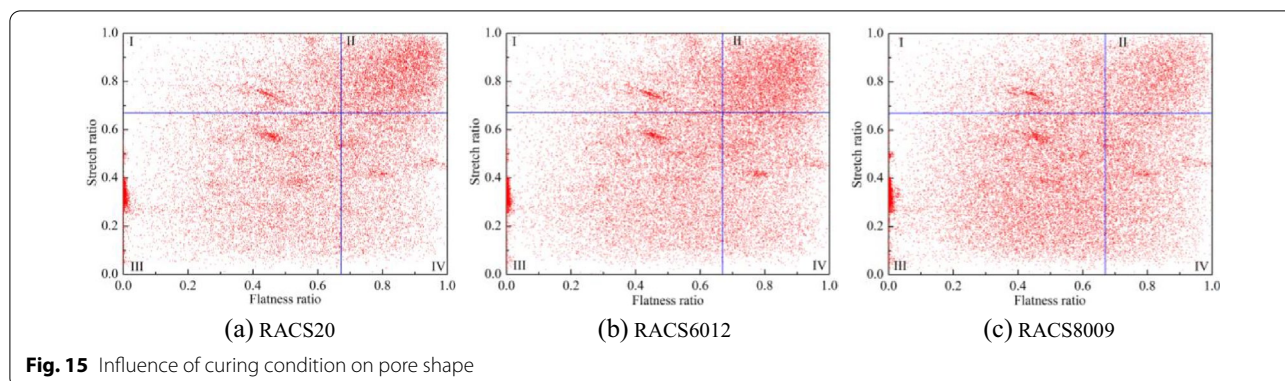


Fig. 15 Influence of curing condition on pore shape

$$Per = \frac{A_g}{A_c} \times 100\%, \tag{3}$$

where A_g is the area of the aggregate on the two-dimensional slice (mm^2) and A_c is the cross-sectional area of the specimen on the two-dimensional slice (mm^2).

Fig. 16 shows the aggregate percentage of RACS, RACS6012, and RACS8009 specimens. The percentage of aggregate has no direct relationship with the curing condition and admixture. From the analysis results, it can be seen that the percentage of recycled aggregate in any section is basically between 30 and 50%, and the average percentage is about 39.7%. The proportions of old mortar and aggregate in recycled aggregate are almost equal, 17.5% and 22.2%, respectively. The actual proportion of recycled aggregate can be obtained by analyzing the composition and percentage of recycled aggregate, which proves that steam curing system will not affect the composition of recycled aggregate concrete. The performance of the old mortar is not only affected by the mix proportion of the original concrete but also further damaged in the crushing process, which adversely affects the quality of RAC, and even the main factor affecting the mechanical properties and durability of recycled aggregate concrete.

3.2.2 Fractal Dimension of Recycled Aggregate

To analyze the contour morphological characteristics of recycled aggregate and old mortar, the fractal dimension is analyzed, as shown in Fig. 17. Recycled aggregate contains aggregate and old mortar, which accounts for the highest percentage in the 2D plane, and its fractal dimension is greater than that of old mortar and aggregate. The proportion of old mortar is slightly lower than that of aggregate, but the fractal dimension is significantly larger than that of aggregate, indicating that the surface morphology of old mortar is more complex, and the surface morphology of aggregate is relatively flat. The complexity of the surface morphology of the old mortar is conducive to the bonding between the old mortar and the mortar in the fresh concrete. However, the complex shape of the old mortar is also easy to contain debris, mud, and other impurities, resulting in some weak links in the interface between the new and old mortar, which increases the dispersion of the mechanical properties of recycled aggregate concrete. Due to the complex surface morphology of old mortar, the compactness of aggregate is small. With the increase of recycled coarse aggregate adhesive mortar content, the overall strength of recycled aggregate concrete is affected and reduced due to the low strength of old mortar. Therefore, it is necessary to clean the recycled

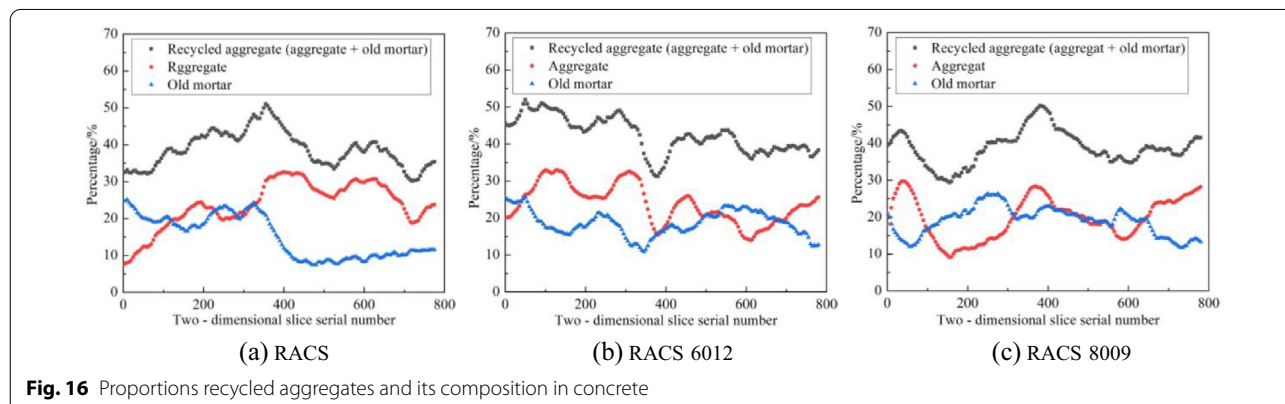
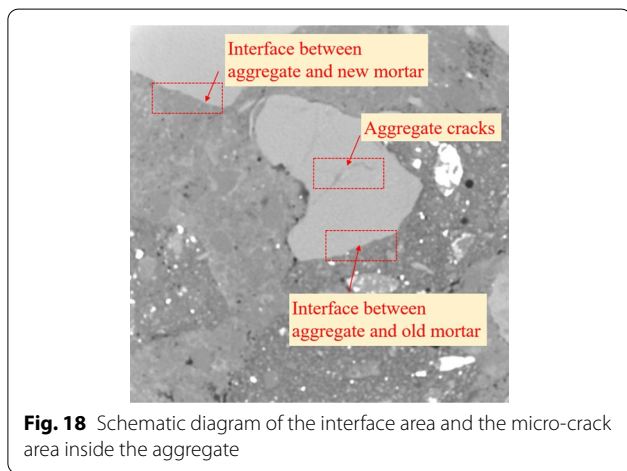
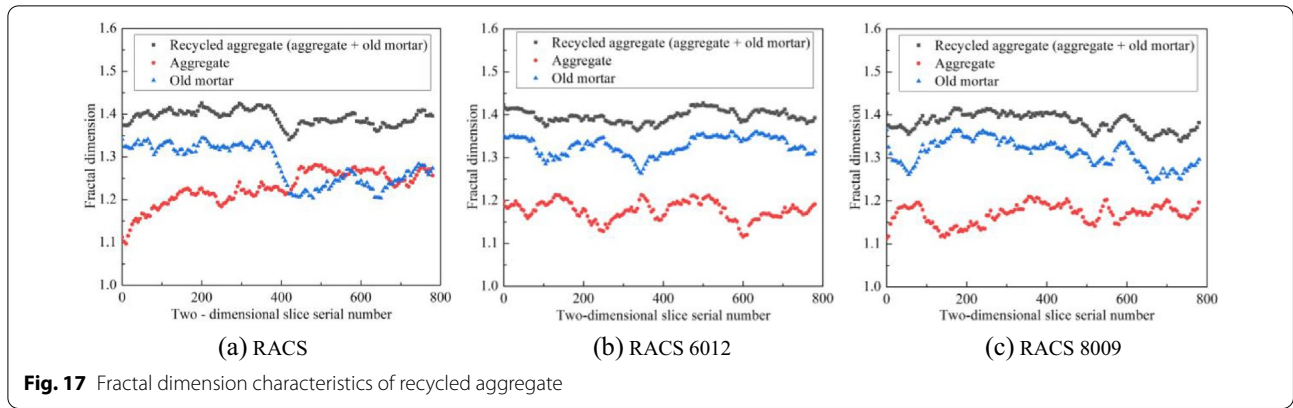


Fig. 16 Proportions recycled aggregates and its composition in concrete



one gray level to another. The jump interval of gray value can be considered as the interface transition zone, and the width of this interval is the thickness of the interface transition zone. The interface transition zone under different curing conditions was measured and analyzed. In order to reduce the measurement error, 5-line segments are drawn at each transition area to calculate and analyze the gray value.

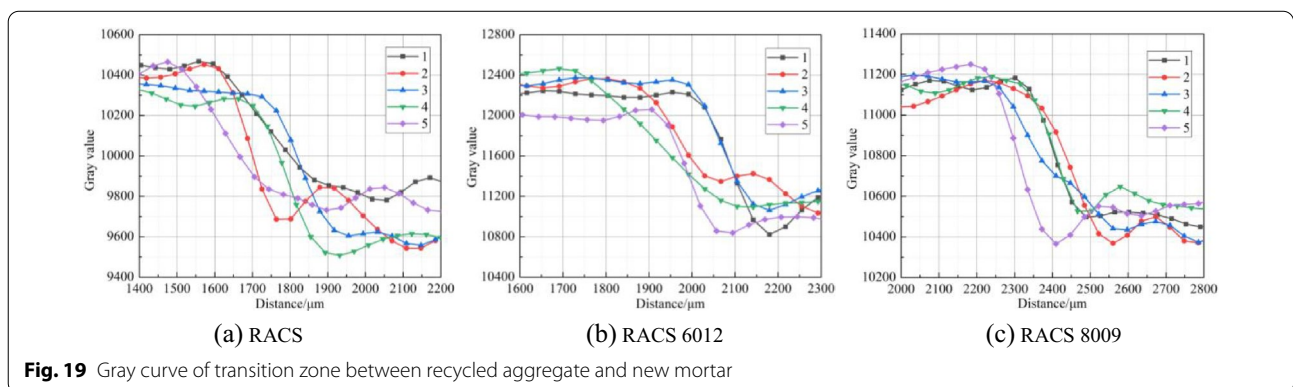
Fig. 18 shows the internal interface transition zone of concrete specimen and micro-cracks in aggregate. A certain number of equidistant line segments are drawn in the selected area, and the gray data of the section are extracted along the line, and the distance across the gray value jump interval is statistically analyzed, so as to obtain the corresponding size of the interface transition zone and the width of micro-cracks in the aggregate.

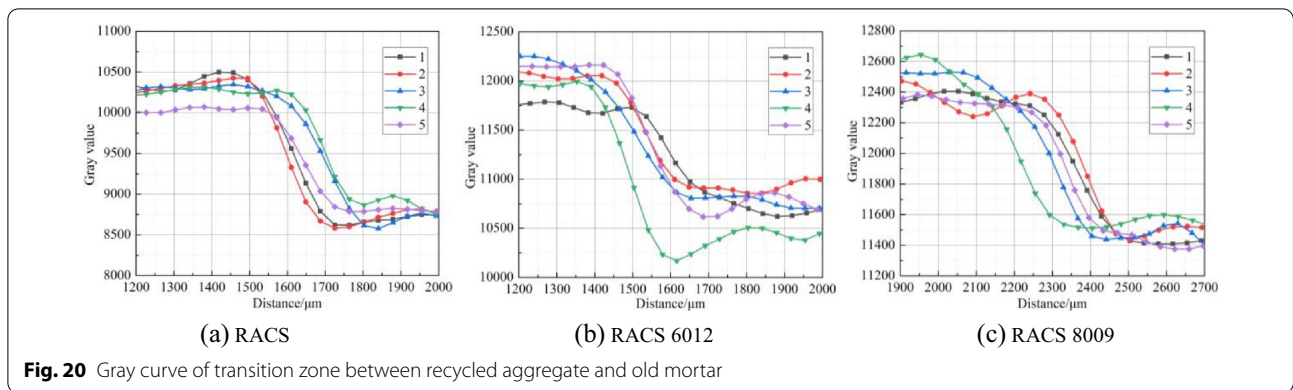
aggregate before use, so as to improve the compactness and mechanical properties of concrete aggregate.

3.3 Interface Transition Zone

On the 2D gray-scale image scanned by X-ray CT, in the area of transition from aggregate to mortar, or from old mortar to new mortar, the gray value will jump from

Figs. 19 and 20 show the gray curves of the transition zone between RA and new and old mortar under different curing conditions. It can be seen from the diagram that the thickness of the interface transition zone can be measured under the accuracy of CT scanning is about 200 μm . Steam curing does not significantly change the thickness of the interface transition zone between aggregate and mortar, and the thickness of the interface



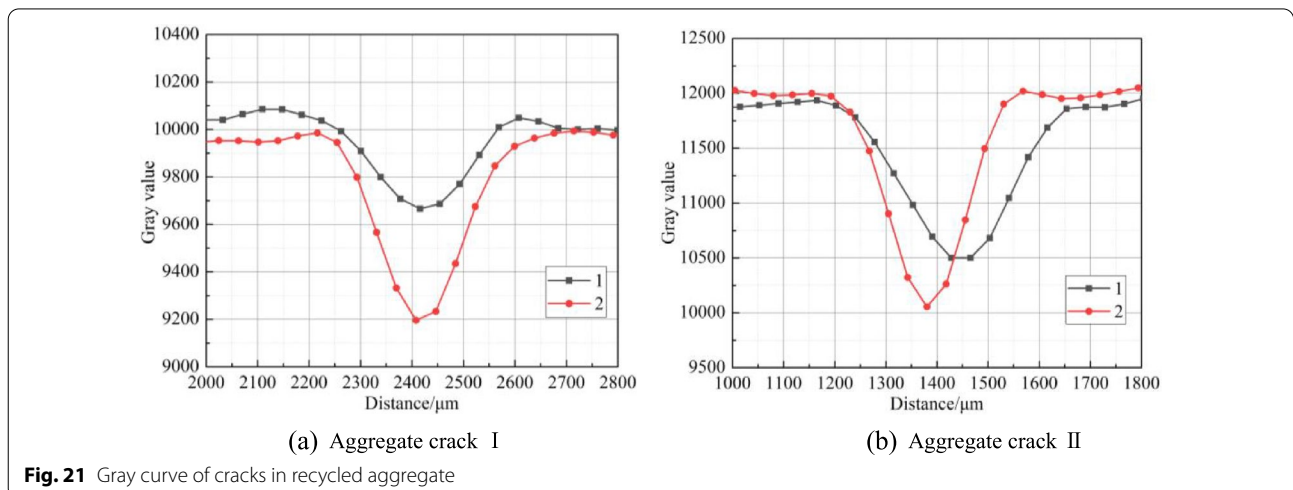


transition zone between aggregate and old and new mortar is similar. The crushing process has caused certain damage to the aggregate in the RA, causing cracks in some aggregates. Two aggregate cracks are randomly selected in the RAC, and two lines are drawn for each crack to calculate the gray value. As shown in Fig. 21, the crack width in the RA is about 300–400 μm. That is because that the surface of recycled aggregate originally contained a large number of pores, which led to stress concentration under the action of external forces, resulting in poor mechanical properties of recycled aggregate and cracks in the crushing process. Due to the existence of these cracks, it may reduce the quality of aggregate and adversely affect the mechanical properties of RAC.

4 Conclusion

In this paper, RCA with admixture of slag power and fly ash and curing condition of steam curing was cast, and X-ray CT was used to analysis meso-structure of RCA. The conclusion is shown as follows:

1. Steam curing not only increases the pore volume in concrete but also makes the pore morphology more complex, and the effect of steaming temperature is greater than that of steaming time, and the fractal dimension increases, the proportion of spherical pores decreases, and the pores develop from spherical to flat and slender.
2. The porosity of each specimen is relatively close, between 2.27% and 2.38%. The porosity is slightly reduced by adding slag powder and fly ash, while the porosity is increased by steam curing at high temperature. The proportion of porosity in the range of 75 μm ~ 300 μm is more than 85%.
3. Based on X-ray CT, the porosity of micron-sized pores in recycled aggregate concrete is about 2.3%, and the proportion of pores with pore size less than 300 μm reaches more than 85%. The thickness of the interface between new and old mortar is about 200 μm, and the crack width in recycled aggregate is about 300~400 μm. This shows that the existence of cracks in recycled aggregate has adverse effects on



the mechanical properties of recycled aggregate concrete.

However, this paper lacks micro and macro research on recycled aggregate concrete of different ages.

Acknowledgements

Not applicable.

Author contributions

YC contributed to conceptualization, validation, and writing—original draft; YN was involved in testing, investigation, and visualization; XC contributed to conceptualization and data curation; WX performed investigation and data analysis; YG was involved in testing and data analysis. All the authors read and approved the final manuscript.

Authors' information

YC is a Lecturer of Architectural Engineering at Jinling Institute of Technology, Nanjing City, Jiangsu Province, China (postal code: 211199). YN is a Senior Engineer of Zhejiang Communications Construction Group Co., Ltd, Hangzhou City, Zhejiang Province, China (postal code: 310051). XC is a Professor in College of Civil and Transportation Engineering at Hohai University, Nanjing City, Jiangsu Province, China (postal code: 210098). WX is a Professor of Architectural Engineering at Jinling Institute of Technology, Nanjing City, Jiangsu Province, China (postal code: 211199). YG is a Ph. D Student in College of Civil and Transportation Engineering at Hohai University, Nanjing City, Jiangsu Province, China (postal code: 210098).

Funding

The work was supported by Jiangsu Industry University Research Cooperation Project (No. 2021059), and Scientific Research Foundation for High-level Talent of Jinling Institute of Technology (No. jit-b-202210).

Availability of data and materials

The data and material are available.

Declarations

Ethics approval and consent to participate

Not applicable.

Consent for publication

All the authors have read the final version of the manuscript and agree to its publication.

Competing interests

The author declare that they have no known competing financial interests or personal relationships that could have appeared to influence the work reported in this paper.

Author details

¹School of Architectural Engineering, Jinling Institute of Technology, Nanjing 211169, China. ²College of Civil and Transportation Engineering, Hohai University, Nanjing 210098, China. ³Zhejiang Communications Construction Group Co., Ltd, Hangzhou 310051, China.

Received: 27 June 2022 Accepted: 1 November 2022

Published online: 20 February 2023

References

- Chandruppa, A. K., & Biligiri, K. P. (2018). Pore structure characterization of pervious concrete using X-ray microcomputed tomography. *Journal of Materials in Civil Engineering*, 30, 04018108. [https://doi.org/10.1061/\(ASCE\)MT.1943-5533.0002285](https://doi.org/10.1061/(ASCE)MT.1943-5533.0002285)
- de Andrade Salgado, F., & de Andrade Silva, F. (2022). Recycled aggregates from construction and demolition waste towards an application on structural concrete: A review. *Journal of Building Engineering*, 52, 104452. <https://doi.org/10.1016/j.jobe.2022.104452>
- Gonzalez-Corominas, A., Etxeberria, M., & Poon, C. S. (2016). Influence of steam curing on the pore structures and mechanical properties of fly-ash high performance concrete prepared with recycled aggregates. *Cement Concrete Composites*, 71, 77–84. <https://doi.org/10.1016/j.cemconcomp.2016.05.010>
- Guo, Y., Chen, X., Chen, B., Wen, R., & Wu, P. (2021). Analysis of foamed concrete pore structure of railway roadbed based on X-ray computed tomography. *Construction and Building Materials*, 273, 121773. <https://doi.org/10.1016/j.conbuildmat.2020.121773>
- Hong, C. W., Jang, H. S., & Jeong, W. K. (2006). Strength and durability properties of concretes using ground granulated blast-furnace slag according to steam curing types. *Journal of Korean Institute of Research Recycling*, 15, 52–59.
- Jun, T., Yuya, S., Tatsuhiko, S., & Michio, S. (2012). Basic study on strength characteristic of fly ash concrete under steam curing. *Cement Science and Concrete Technology*. <https://doi.org/10.14250/cement.66.359>
- Kim, B. K., Lee, J. S., Lee, G. P., Chang, S. H., & Bae, G. J. (2011). Mechanical characteristics of high-performance concrete shield segment containing ground granulated blast furnace slag and their improvement by steam curing. *Journal of Korean Tunnel Underground Space Association*, 13, 233–242.
- Kou, S. C., & Poon, C. S. (2008). Mechanical properties of 5-year-old concrete prepared with recycled aggregates obtained from three different sources. *Magazine of Concrete Research*, 60, 57–64. <https://doi.org/10.1680/mac.2007.00052>
- Lee, M. K., Kim, K. S., Lee, K. H., & Jiang, S. H. (2005a). An experimental study on the strength of recycled concrete with steam curing. *Journal of Korea Institute of Building Construction*, 5, 89–95. <https://doi.org/10.5345/JKIC.2005.5.2.089>
- Lee, M. K., Kim, K. S., Lee, K. H., & Jiang, S. H. (2005b). Strength of recycled concrete with furnace slag cement under steam curing condition. *Journal of Korea Concrete Institute*, 17, 613–620. <https://doi.org/10.4334/JKCI.2005.17.4.613>
- Li, M., Wang, Q., & Yang, J. (2017). Influence of steam curing method on the performance of concrete containing a large portion of mineral admixtures. *Advanced Materials in Science Engineering*. <https://doi.org/10.1155/2017/9863219>
- Liu, X., Wang, C., Deng, Y., & Cao, F. (2016). Computation of fractal dimension on conductive path of conductive asphalt concrete. *Construction and Building Materials*, 115, 699–704. <https://doi.org/10.1016/j.conbuildmat.2016.04.051>
- Ma, Z., Shen, J., Wang, C., & Wu, H. (2022). Characterization of sustainable mortar containing high-quality recycled manufactured sand crushed from recycled coarse aggregate. *Cement and Concrete Composites*, 132, 104629. <https://doi.org/10.1016/j.cemconcomp.2022.104629>
- McGinnis, M. J., Davis, M., de la Rosa, A., Brad, D. W., & Yahya, C. K. (2017). Strength and stiffness of concrete with recycled concrete aggregates. *Construction and Building Materials*, 154, 258–269. <https://doi.org/10.1016/j.conbuildmat.2017.07.015>
- Ouyang, J., Liu, K., Sun, D., Xu, W., Wang, A., & Ma, R. (2022). A focus on Ca²⁺ supply in microbial induced carbonate precipitation and its effect on recycled aggregate. *Journal of Building Engineering*, 51, 104334. <https://doi.org/10.1016/j.jobe.2022.104334>
- Poon, C. S., Kou, S. C., & Chan, D. (2006). Influence of steam curing on hardened properties of recycled aggregate concrete. *Magazine of Concrete Research*, 58, 289–299. <https://doi.org/10.1680/mac.2006.58.5.289>
- Ramezaniapou, A. M., Esmarili, K., Ghahari, S. A., & Ramezaniapour, A. A. (2014). Influence of initial steam curing and different types of mineral additives on mechanical and durability properties of self-compacting concrete. *Construction and Building Materials*, 73, 187–194. <https://doi.org/10.1016/j.conbuildmat.2014.09.072>
- Shi, J., Liu, B., Wu, X., Qin, J., Jiang, J., & He, Z. (2020a). Evolution of mechanical properties and permeability of concrete during steam curing process. *Journal of Building Engineering*, 33, 101796. <https://doi.org/10.1016/j.jobe.2020.101796>
- Shi, J., Liu, B., Zhou, F., Shen, S., Dai, J., Ji, R., & Tan, J. (2020b). Heat damage of concrete surfaces under steam curing and improvement measures. *Construction and Building Materials*, 252, 119104. <https://doi.org/10.1016/j.conbuildmat.2020.119104>

- Suryawanshi, S. R., Singh, B., & Bhargava, P. (2015). Characterization of recycled aggregate concrete. *Advanced in Structural Engineering*. https://doi.org/10.1007/978-81-322-2187-6_139
- Tan, K., & Zhu, J. (2017). Influences of steam and autoclave curing on the strength and chloride permeability of high strength concrete. *Materials and Structures*, 50, 1–9. <https://doi.org/10.1617/s11527-016-0913-6>
- Wang, C., Xiao, J., Liu, W., & Ma, Z. (2022). Unloading and reloading stress-strain relationship of recycled aggregate concrete reinforced with steel/polypropylene fibers under uniaxial low-cycle loadings. *Cement and Concrete Composites*, 131, 104597. <https://doi.org/10.1016/j.cemconcomp.2022.104597>
- Yang, J., Hu, H., He, X., Su, Y., Wang, Y., Tan, H., & Pan, H. (2021). Effect of steam curing on compressive strength and microstructure of high-volume ultrafine fly ash cement mortar. *Construction and Building Materials*, 266, 120894. <https://doi.org/10.1016/j.conbuildmat.2020.120894>

Publisher's Note

Springer Nature remains neutral with regard to jurisdictional claims in published maps and institutional affiliations.

Submit your manuscript to a SpringerOpen[®] journal and benefit from:

- ▶ Convenient online submission
- ▶ Rigorous peer review
- ▶ Open access: articles freely available online
- ▶ High visibility within the field
- ▶ Retaining the copyright to your article

Submit your next manuscript at ▶ [springeropen.com](https://www.springeropen.com)
